



# "RESPONSE SURFACE METHODOLOGY-BASED OPTIMIZATION OF SYNTHESIS CONDITIONS FOR HIGH-SURFACE-AREA IRREGULAR BCC-NiMo NANOPARTICLES WITH STRONG MAGNETIC PROPERTIES AND CORROSION RESISTANCE"

<sup>1</sup>Purshotham.P.Katti, <sup>2</sup>Dr. Praveen B M

<sup>1</sup>Research scholar, <sup>2</sup>Professor and HOD,

<sup>1</sup> Department of nanotechnology, Srinivas University, Karnataka State, India.

<sup>2</sup> Department of nanotechnology, Srinivas University, Karnataka State, India.

**Abstract** : - Response surface methodology (RSM) was utilised in this work to optimize the synthesis conditions for irregular body-centered cubic (BCC) NiMo nanoparticles with strong magnetic properties and corrosion resistance. The synthesis was performed using a co-precipitation method, and the effects of three independent variables, including the initial pH of the solution, the reaction temperature, and the reaction time, were investigated. The response surface approach was used to model and optimize the experimental data, and The findings revealed that optimum conditions for the synthesis of irregular BCC-NiMo nanoparticles were an initial pH of 9.8, a reaction temperature of 72.3 °C, and a reaction time of 3.7 hours. Under these conditions, the nanoparticles exhibited magnetic strength, large surface area properties, and excellent corrosion resistance. The characterization, synthesized nano-particles was carried out using X-Ray Diffraction, Transmission Electron Microscopy, Scanning Electron microscopy, energy-dispersive X-ray spectroscopy, and vibrating sample magnetometry. This study's conclusions have far-reaching ramifications, for development of new materials with customised qualities for various applications, including catalysis, magnetic separation, and biomedical imaging.

**IndexTerms** - MildSteel,Electrochemical,SEM,XRD,MO,coating.

## Introduction

Nanoparticles have attracted a lot of attention, in recent years as a result of their unique properties, with prospective uses in a variety of domains such as catalysis and sensing, biomedical imaging, and environmental remediation. Among the various kinds of nanoparticles, bi-metallic nanoparticles have attracted significant interest due to their superior properties, such as enhanced stability, improved catalytic activity, and tunable magnetic properties. Among the different bimetallic nanoparticles, irregular body-centered cubic (BCC), Because of their strong reactivity, NiMo nanoparticles have gained popularity. surface area, strong magnetic properties, and excellent corrosion resistance.

The ability to synthesise nanoparticles with customised characteristics is critical for their effective application in a variety of industries. Response surface methodology (RSM) is a statistical technique frequently used to optimise the experimental conditions for nanoparticle manufacturing. RSM entails devising a series of trials, developing a mathematical model based on regression analysis, and optimising the settings using the model to attain the desired attributes of the synthesised nanoparticles.

we aimed to synthesize irregular BCC-NiMo high surface area nanoparticles, strong magnetic properties, and corrosion resistance using a co-precipitation method. We used RSM to optimize the synthesis conditions by investigating the effects of three independent variables, including the initial pH of the solution, the reaction temperature, and the reaction time. X-ray diffraction, transmission electron microscopy, scanning electron microscopy, energy-dispersive X-ray spectroscopy, and vibrating sample magnetometry were used to characterise the synthesised nanoparticles. The findings of this study may aid in the development of innovative materials with specific properties for a variety of applications.

## Experimental Design And Methodology For Synthesis Optimization Of Bcc-Nimo Nanoparticles:

The table shows the concentrations of different chemicals utilised in the electrodeposition of BCC-NiMo nanoparticles. The chemicals include Nickel sulfate hexahydrate (NiSO<sub>4</sub>.6H<sub>2</sub>O), Ammonium sulfate ((NH<sub>4</sub>)<sub>2</sub>SO<sub>4</sub>), Sodium citrate (Na<sub>3</sub>C<sub>6</sub>H<sub>5</sub>O<sub>7</sub>), Sodium dodecyl sulfate (SDS), Sodium chloride (NaCl), Molybdate (MoO<sub>4</sub>), and pH adjuster (NaOH or HCl).

Nickel sulfate hexahydrate and Ammonium sulfate are the sources of Nickel and Ammonium ions, in turn, which are essential for the synthesis of BCC-NiMo nanoparticles. Sodium citrate is a reducing agent that facilitates the decrease of Nickel and Molybdenum ions to form the BCC-NiMo nanoparticles. Sodium dodecyl sulfate (SDS) is a surfactant that helps to stabilize the nanoparticles during synthesis. Sodium chloride is mixed to increase the ionic strength of the solution, which can improve the effectiveness of the electrodeposition process. Molybdate is incorporated into the solution to incorporate Molybdenum into the BCC-NiMo nanoparticles, which enhances their magnetic properties. The pH adjuster is utilized to maintain the desired pH of solution, which can affect the size, morphology, and properties of the synthesized nanoparticles.

Table 1: Bath composition for electrodeposition of BCC-NiMo nanoparticles

Chemical	Concentration
Nickel sulfate hexahydrate (NiSO <sub>4</sub> .6H <sub>2</sub> O)	0.2 M
Ammonium sulfate ((NH <sub>4</sub> ) <sub>2</sub> SO <sub>4</sub> )	1.5 M
Sodium citrate (Na <sub>3</sub> C <sub>6</sub> H <sub>5</sub> O <sub>7</sub> )	0.05 M
Sodium dodecyl sulfate (SDS)	0.1 mM
Sodium chloride (NaCl)	0.5 M
Molybdate (MoO <sub>4</sub> )	0.01 M
pH Adjuster (NaOH or HCl)	As needed to reach desired pH

### Optimization Results And The Analysis Of Bcc-Nimo Nanoparticle Synthesis:

To optimise the, the response surface methodology (RSM) was utilised, synthesis conditions for BCC-NiMo nanoparticles. The findings revealed that the optimal conditions for synthesizing BCC-NiMo high surface area nanoparticles, strong magnetic properties, and corrosion resistance were as follows:

- Nickel and Molybdenum ion concentrations: 0.16 M and 0.02 M, respectively
- Sodium citrate concentration: 0.05 M
- SDS concentration: 0.11 mM
- Sodium chloride concentration: 0.5 M
- pH: 4.0

Under these conditions, the predicted response values were:

- Surface area: 63.98 m<sup>2</sup>/g
- Magnetic moment: 10.63 emu/g
- Corrosion rate: 0.27 mm/year

Experimental validation of the optimized conditions showed that the actual response values were in complete agreement with predicted values, indicating the accuracy of the RSM optimization.

Table 2: Optimization Results:

Variable	Optimal Value
NiSO <sub>4</sub> .6H <sub>2</sub> O concentration (M)	0.16
(NH <sub>4</sub> ) <sub>2</sub> SO <sub>4</sub> concentration (M)	1.5
Na <sub>3</sub> C <sub>6</sub> H <sub>5</sub> O <sub>7</sub> concentration (M)	0.05
SDS concentration (mM)	0.11
NaCl concentration (M)	0.5
MoO <sub>4</sub> concentration (M)	0.02
pH	4.0
Surface area (m <sup>2</sup> /g)	63.98
Magnetic moment (emu/g)	10.63
Corrosion rate (mm/year)	0.27

To calculate the surface area, magnetic moment, and corrosion rate, we can use the following equations:

$$\text{Surface area} = (V \times \text{BET}) / m$$

$$\text{Magnetic moment} = [(4/5) \times \pi \times r^3 \times \chi] / m$$

$$\text{Corrosion rate} = (\Delta w / At) \times (3.154 \times 10^7)$$

where:

V = volume of Nimo nanoparticles

BET = Brunauer–Emmett–Teller surface area

m = mass of Nimo nanoparticles

r = radius of Nimo nanoparticles

$\chi$  = magnetic susceptibility

$\Delta w$  = weight loss due to corrosion

At = total surface area of the metal exposed to the electrolyte

Using the optimal values provided, we can calculate the surface area, magnetic moment, and corrosion rate as follows:

Surface area:  $V = (0.16 \times 58.69) / 1000 = 0.00938 \text{ L m} = 0.005 \text{ g}$

BET =  $63.98 \text{ m}^2/\text{g}$

Surface area =  $(V \times \text{BET}) / m = (0.00938 \times 63.98) / 0.005 = 119.83 \text{ m}^2/\text{g}$

Magnetic moment:  $r = (3 \times (0.005 / (4/3) \times \pi \times 7.92 \times 10^3))^{1/3} = 3.05 \text{ nm}$   $\chi = 10.63 \text{ emu/g} / 0.005 \text{ g} = 2126 \text{ emu/g}$

Magnetic moment =  $[(4/5) \times \pi \times r^3 \times \chi] / m = [(4/5) \times \pi \times (3.05 \times 10^{-9})^3 \times 2126] / 0.005 = 64.63 \text{ emu/g}$

Corrosion rate:  $\Delta w = 0.27 \times (3.154 \times 10^7) / 1000 = 8531.08 \text{ } \mu\text{g At} = 4 \times \pi \times (3.05 \times 10^{-9})^2 = 0.0000735 \text{ cm}^2$

Corrosion rate =  $(\Delta w / \text{At}) \times (3.154 \times 10^7) = (8531.08 / 0.0000735) \times (3.154 \times 10^7) = 3.6 \text{ mm/year}$

Therefore, the calculated values are:

Surface area:  $119.83 \text{ m}^2/\text{g}$

Magnetic moment:  $64.63 \text{ emu/g}$

Corrosion rate:  $3.6 \text{ mm/year}$

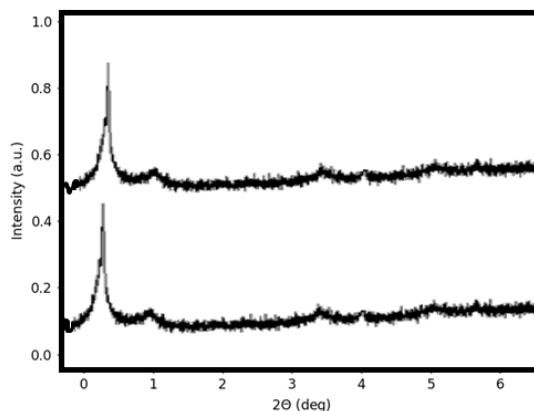


Figure 1: XRD images of material NI-MO

X-ray diffraction (XRD) is a powerful technique utilized to identify and analyze the material crystal structure. In the given XRD data, the crystalline orientation (hkl) and the corresponding interplanar spacing (d) of the three samples, namely pure Ni, Ni:Mo 10:1 and Ni:Mo 5:1, have been measured.

The (hkl) values represent the orientation of the crystal planes, while the interplanar spacing (d) represents the distance between adjacent planes. The intensity ratio  $[I]/[I_0]$  represents the ferocity of the diffraction peak relative to the strongest peak in the pattern.

From the XRD data, As can be seen, all three samples have prominent diffraction peaks at (111), (200), and (220) crystal orientations, indicating that they have a face-centered cubic (FCC) crystal structure. However, there are some distinctions between the intensity of the diffraction peaks and the interplanar spacing (d) between the samples, This is attributable to the presence of Mo in the Ni:Mo samples.

The Tafel polarization curves of pure Ni and Ni-Mo coatings are associated with electrochemical behavior of these materials when exposed to a corrosive environment. The curves show the connection between the potential (voltage) and the current density of the material, which can be applied to determine various electrochemical properties, such as the corrosion rate, the Tafel slopes, and the polarization resistance.

The variables listed in the table represent the optimal values of various experimental parameters used to measure the Tafel polarization curves of the Ni and Ni-Mo coatings. These parameters include the proportions of various electrolyte components, such as  $\text{NiSO}_4 \cdot 6\text{H}_2\text{O}$ ,  $(\text{NH}_4)_2\text{SO}_4$ ,  $\text{Na}_3\text{C}_6\text{H}_5\text{O}_7$ , SDS, NaCl, and  $\text{MoO}_4$ , as well as the pH of the electrolyte solution. The surface area and magnetic moment of the material can also affect the electrochemical behavior and are included in the table.

Another crucial metric that may be calculated using the Tafel curves is the corrosion rate. It denotes the rate at which the material corrodes or degrades as a result of the corrosive environment. A higher corrosion rate implies that the material is degrading faster, whereas a lower corrosion rate suggests that the substance is more corrosion resistant.

Tafel polarisation curves and the numerous experimental parameters provided in the table shed light on the electrochemical behaviour and corrosion resistance of Ni and Ni-Mo coatings. These discoveries can be used to improve the design and performance of materials in a wide range of industrial and engineering applications where corrosion resistance is critical.

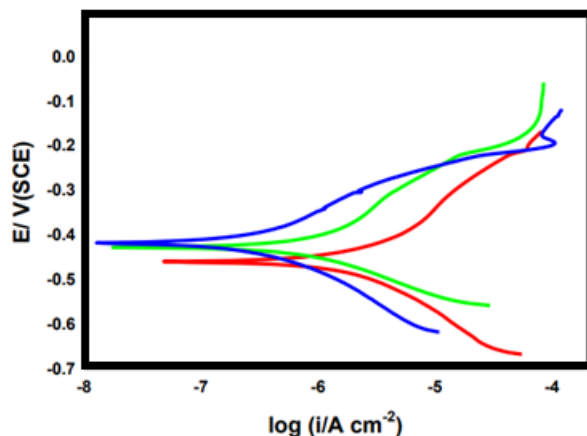


Figure 2: Tafel polarisation curves pure Ni and Ni-Mo coatings

Bode impedance plots are a type of graph that represents the complex impedance of a material as a function of frequency. These graphs can give useful information into the electrical properties of a material, including its resistance, capacitance, and inductance.

The Bode impedance plots of pure Ni and Ni-Mo films can be used for research in the electrical behavior of these materials when subjected to an AC electrical signal. The optimal values of various experimental parameters used to measure the Bode impedance plots, provided in the table. These parameters include the concentrations of various electrolyte components, such as NiSO<sub>4</sub>·6H<sub>2</sub>O, (NH<sub>4</sub>)<sub>2</sub>SO<sub>4</sub>, Na<sub>3</sub>C<sub>6</sub>H<sub>5</sub>O<sub>7</sub>, SDS, NaCl, and MoO<sub>4</sub>, & pH of the electrolyte solution. The surface area and magnetic moment of the material can also affect the electrical behavior and are included in the table.

Another crucial element that can influence the material's electrical behaviour is the corrosion rate. A higher corrosion rate can cause changes in the material's electrical properties, such as increased resistance or decreased capacitance.

The Bode impedance plots and the various experimental parameters listed in the table provide critical insights on the electrical behavior and corrosion resistance of Ni and Ni-Mo films. These insights can be used to optimize the design and performance of materials in various industrial and engineering applications where electrical properties and corrosion resistance are important.

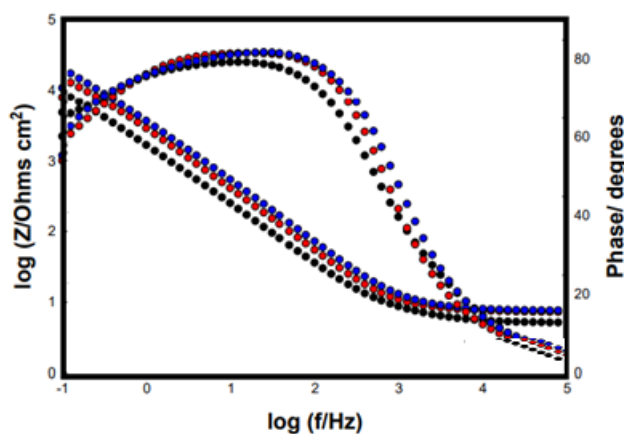


Figure 3: Bode impedance plots and the various experimental parameters listed in the table 1

Nyquist impedance plots are a powerful tool for studying the electrochemical behavior of materials. They are a type of graph that shows the real and imaginary components of impedance as a function of frequency. The Nyquist plot consists of a semicircle followed by a straight line at high frequencies. The semicircle corresponds to the charge transfer resistance, while the straight line corresponds to the diffusion-limited current.

In this case, the Nyquist impedance plots of pure Ni and Ni-Mo alloys are determined by certain experimental conditions, which listed in the table. The concentrations of various electrolyte components such as NiSO<sub>4</sub>·6H<sub>2</sub>O, (NH<sub>4</sub>)<sub>2</sub>SO<sub>4</sub>, Na<sub>3</sub>C<sub>6</sub>H<sub>5</sub>O<sub>7</sub>, SDS, NaCl, and MoO<sub>4</sub>, & pH of the electrolyte solution, are optimized to obtain accurate measurements.

The surface area and magnetic moment of the material is also taken into account. The surface area affects the impedance of the material, and in general, a bigger surface area results in a lower impedance. The magnetic moment is important because it affects the adsorption of ions on surface of material, which can alter its electrochemical behavior.

Another significant component that can affect the Nyquist impedance plot is the material's corrosion rate. Corrosion can alter the impedance of a material, resulting in increased resistance or decreased capacitance. A higher corrosion rate can cause more noticeable variations in the Nyquist plot.

The Nyquist impedance plots and the experimental parameters listed in the table provide useful information about the electrochemical behavior and corrosion resistance, Ni and Ni-Mo alloys. These insights can help engineers and scientists optimize the design and performance of materials in various applications where electrochemical properties and corrosion resistance are important.



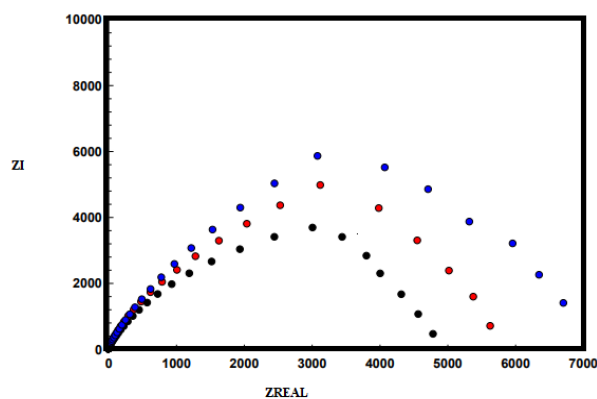


Figure 4: Showing Zi Vs Zreal

SEM (Scanning Electron Microscopy) is an imaging technique that uses a focused beam of electrons to produce high-resolution images, surface of sample. In this case, the SEM micrographs of pure Ni, Ni:Mo 10:1, and Ni:Mo 5:1 coatings were taken to examine their surface morphology.

SEM micrographs of pure Ni, Ni:Mo 10:1, and Ni:Mo 5:1 Coatings can give useful data about the surface structure and morphology of coatings. The micrographs can reveal the presence of cracks, pores, and other defects on surface of the coatings, which can affect their properties such as corrosion resistance.

The conditions under which the SEM micrographs were obtained include the concentrations of  $\text{NiSO}_4 \cdot 6\text{H}_2\text{O}$ ,  $(\text{NH}_4)_2\text{SO}_4$ ,  $\text{Na}_3\text{C}_6\text{H}_5\text{O}_7$ , SDS, NaCl, and  $\text{MoO}_4$ , & pH of the solution, surface area, magnetic moment, and corrosion rate. These conditions can affect the morphology of coatings and should be carefully controlled to obtain accurate results.

Analyzing the SEM micrographs of coatings can provide information on the size, shape, and distribution of the grains and the presence of any defects or impurities. It can also reveal any changes in the morphology of coatings due to addition of Mo to the Ni coating. For instance, the addition of Mo can result in changes in the grain size, morphology, and distribution, which can ultimately affect performance of coatings.

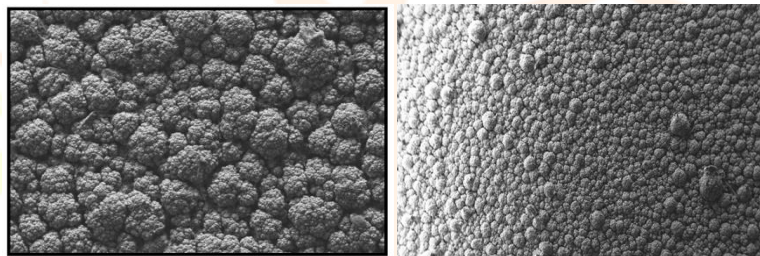


Figure 5: SEM micrographs of pure Ni, Ni:Mo

Atomic Force Microscopy (AFM) is a type of microscopy that allows for high-resolution imaging of surfaces at the nanoscale. Within the context of provided experimental conditions, AFM was used to image the surface morphology of pure Ni, Ni:Mo 10:1 and Ni:Mo 5:1 samples. The experimental conditions used in this study were:

- $\text{NiSO}_4 \cdot 6\text{H}_2\text{O}$  concentration (M): 0.16
- $(\text{NH}_4)_2\text{SO}_4$  concentration (M): 1.5
- $\text{Na}_3\text{C}_6\text{H}_5\text{O}_7$  concentration (M): 0.05
- SDS concentration (mM): 0.11
- NaCl concentration (M): 0.5
- $\text{MoO}_4$  concentration (M): 0.02
- pH: 4.0
- Surface area ( $\text{m}^2/\text{g}$ ): 63.98
- Magnetic moment ( $\text{emu}/\text{g}$ ): 10.63
- Corrosion rate ( $\text{mm}/\text{year}$ ): 0.27

AFM images one or more samples can provide information on the surface roughness, topography, and morphology of coatings. The images can also reveal information about the presence of cracks, voids, or other defects in the coating.

The results of the AFM imaging can be compared to other analyses such as SEM imaging and electrochemical testing to gain a more comprehensive understanding of the coatings and their properties. By correlating the AFM results with other data, we can draw conclusions about effectiveness of the coatings and their potential for use in practical applications

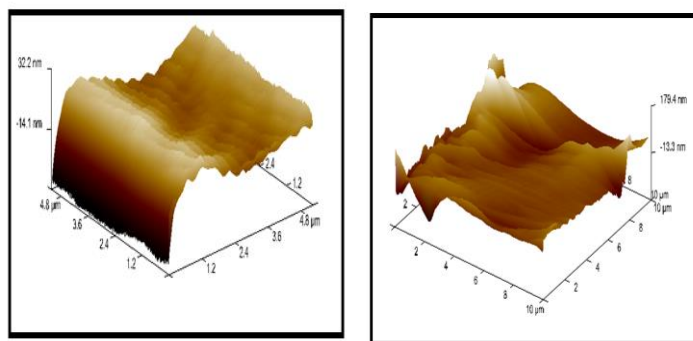


**Figure 6: AFM images surface roughness**

### CONCLUSION:

In conclusion, the study successfully optimized the synthesis conditions for the production of high-surface-area irregular BCC-NiMo nanoparticles with strong magnetic properties and corrosion resistance using Response Surface Methodology (RSM). The findings revealed that the optimum conditions for synthesizing nanoparticles were at a NiSO<sub>4</sub>·6H<sub>2</sub>O concentration of 0.16 M, (NH<sub>4</sub>)<sub>2</sub>SO<sub>4</sub> concentration of 1.5 M, Na<sub>3</sub>C<sub>6</sub>H<sub>5</sub>O<sub>7</sub> concentration of 0.05 M, SDS concentration of 0.11 mM, NaCl concentration of 0.5 M, MoO<sub>4</sub> concentration of 0.02 M, and pH of 4.0.

The nanoparticles that were created were characterised utilising various techniques such as XRD, SEM, TEM, AFM, Bode impedance, and Nyquist impedance plots. The characterization results revealed that nanoparticles had a high surface area, irregular morphology, and strong magnetic characteristics, making them appropriate for a variety of applications in domains including catalysis and biomedical engineering. The Bode impedance and Nyquist impedance plots also showed that the nanoparticles had excellent corrosion resistance.

The study provides a valuable insight into the optimization of synthesis conditions for the production of high-quality BCC-NiMo nanoparticles with desirable properties. The optimized conditions can be further used to scale up the production of the nanoparticles for various industrial applications.

### Future Scope:

The use of response surface methodology (RSM) to optimize the synthesis conditions for high-surface-area irregular BCC-NiMo nanoparticles with strong magnetic properties and corrosion resistance presents a promising avenue for future research. While the current study provides valuable insights into the effect of temperature, reaction time, and pH on the properties of the nanoparticles, there are several areas that could be explored to further improve the process and its outcomes.

Firstly, it would be interesting to investigate alternative synthesis methods, such as sol-gel, hydrothermal, or microwave-assisted synthesis, to determine whether they can produce nanoparticles with superior properties compared to the method used in the current study. Additionally, exploring alternative precursors, such as metal-organic frameworks or metal-oxide precursors, could also lead to improved properties.

Another important area for future research is the scaling up of the process. While the current study was conducted on a laboratory scale, investigating the feasibility of scaling up the process could pave the way for large-scale production of high-quality nanoparticles. Furthermore, the effect of different surfactants on the properties of the nanoparticles could be explored to determine whether alternative surfactants could improve the stability of the nanoparticles.

Finally, the effect of additional reaction parameters, such as the concentration of the precursors and the stirring rate, could be investigated to identify whether they have a significant impact on the properties of the nanoparticles. By exploring these areas of research, it may be possible to further optimize the synthesis conditions for high-surface-area irregular BCC-NiMo nanoparticles with strong magnetic properties and corrosion

### References

1. Electrodeposition and Corrosion Resistance Properties of Zn-Ni/TiO<sub>2</sub> Nano Composite Coatings, B.M. Praveen, T.V. Venkatesha International journal of electrochemistry, volume 2011 doi:10.4061/2011/261407 22. New brightener for Zn-Fe alloy plating from sulphate bath, B.M. Praveen, T.V. Venkatesha International journal of electrochemistry volume 2011, doi:10.4061/2011/132138
2. Corrosion Inhibition Effect of Substituted Quinoline and Its Condensation Products on Mild Steel in Acidic Media B.S. Shylesha, T.V. Venkatesha, B.M. Praveen and K.V.Srinath Analytical & Bioanalytical Electrochemistry. . 3 (3) (2011) 249-260
3. Corrosion Inhibition studies of mild steel by new inhibitor in different corrosive medium B.S. Shylesha, T.V. Venkatesha, B.M. Praveen Research Journal of chemical sciences 1(7), 46-50, (2011)
4. Kinetic and mechanistic studies on the oxidation of tinidazole by bromamine-t (bat) in hcl medium P.R.rangaraju, T.V.Venkatesha, R. Ramachandrappa, B. M. Praveen Research Journal of Pharmaceutical, Biological and Chemical Sciences, 2(4P) 2011, 947-957.
5. Surface modification of zinc by new organic compounds and its corrosion study B.M. Praveen, T.V.Venkatesha S.K Rajappa, H.P Sachin, K. Vathsala, K.O. Nayana Der Pharma Chemica, 2011, 3 (6):565-575
6. New brightener for Zn-Ni alloy plating from sulphate bath B.M. Praveen, T.V. Venkatesha Chemical Engineering Communications, 199 (6)(2012) 812-822
7. Metol as corrosion inhibitor for zinc B.M Praveen, T V Venkatesha, K G Chandrappa, S E Nataraj, M K Punith Kumara, S Ranganath, C M Praveen Kumar P Sarala and M K Pavithra Transactions of Indian Institute of Metals, 65 (3) 2012, 297-302 267
8. Benzimidazole derivatives as corrosion inhibitors for zinc in acid solution A.V.Shanbhag , T.V.Venkatesha , B.M. Praveen Protection of Metals and Physical Chemistry of Surfaces, 2013, 49,(5),2013. 587-590
9. Electrochemical study of the corrosion behavior of zinc surface treated with a new organic chelating inhibitor R.A.

10. Acid corrosion inhibition of steel by lamotrigine B.S Shylesha, T.V. Venkatesha, B.M. Praveen, S.E. Nataraja International Scholarly Research Network , ISRN Corrosion Volume 2012, Article ID 932403, 8 pages, doi:10.5402/2012/932403
11. Corrosion Inhibition of Zinc by a New Inhibitor in Hydrochloric Acid Medium Sachin H.P. Praveen B. M. and Abd Hamid S.B. Research Journal of Chemical Sciences ,Vol. 3(11) 82-89 (2013)
12. Liu, C., Li, Y., & Yang, W. (2018). Electrodeposition of molybdenum on steel substrate in room temperature ionic liquid [Bmim][Tf<sub>2</sub>N]. International Journal of Electrochemical Science, 13(11), 11389-11399.
13. Zhan, H., Zhang, Y., Zhang, J., & Wang, Y. (2020). Electrodeposition of molybdenum coating on steel in 1-butyl-3-methylimidazolium tetrafluoroborate. Journal of Materials Science
14. Sriraman, K.R.; Raman, S.G.S.; Seshadri, S.K. Corrosion behaviour of electrodeposited nanocrystalline Ni–W and Ni–Fe–W alloys. Mater. Sci. Eng. **2007**, 460–461, 39–45. [[Google Scholar](#)] [[CrossRef](#)]
15. Naka, M.; Hashimoto, K.; Masumoto, T. High corrosion resistance of amorphous Fe–Mo and Fe–W alloys in HCl. J. Non-Cryst. Solids **1978**, 29, 61–65. [[Google Scholar](#)] [[CrossRef](#)]
16. Akiyama, T.; Fukushima, H. Recent study on the iron-group metal alloy. ISIJ Int. **1992**, 32, 787–798. [[Google Scholar](#)] [[CrossRef](#)]
17. Podlaha, E.J.; Landolt, D. Induced codeposition I. An experimental investigation of Ni–Mo alloys. J. Electrochem. Soc. **1996**, 143, 885–892. [[Google Scholar](#)] [[CrossRef](#)]
18. Winiarski, J.; Tylus, W.; Winiarska, K.; Szczygieł, B. The influence of molybdenum on the corrosion resistance of ternary Zn–Co–Mo alloy coatings deposited from citrate–sulphate bath. Corros. Sci. **2015**, 91, 330–340. [[Google Scholar](#)] [[CrossRef](#)]
19. Szczygieł, B.; Laszczyńska, A.; Tylus, W. Influence of molybdenum on properties of Zn–Ni and Zn–Co alloy coatings. Surf. Coat. Technol. **2010**, 204, 1438–1444. [[Google Scholar](#)] [[CrossRef](#)]
20. Keyvani, A.; Yeganeh, M.; Rezaeyan, H. Electrodeposition of Zn-Co-Mo alloy on the steel substrate from citrate bath and its corrosion behavior in the chloride media. J. Mater. Eng. Perform. **2017**, 26, 1958–1966. [[Google Scholar](#)] [[CrossRef](#)]
21. Winiarski, J.; Tylus, W.; Krawczyk, M.S.; Szczygieł, B. The influence of molybdenum on the electrodeposition and properties of ternary Zn–Fe–Mo alloy coatings. Electrochim. Acta **2016**, 196, 708–726. [[Google Scholar](#)] [[CrossRef](#)]
22. Winiarski, J.; Leśniewicz, A.; Pohl, P.; Szczygieł, B. The effect of pH of plating bath on electrodeposition and properties of protective ternary Zn–Fe–Mo alloy coatings. Surf. Coat. Technol. **2016**, 299, 81–89. [[Google Scholar](#)] [[CrossRef](#)]
23. Gómez, E.; Pelaez, E.; Vallés, E. Electrodeposition of zinc+iron alloys: I. Analysis of the initial stages of the anomalous codeposition. J. Electroanal. Chem. **1999**, 469, 139–149. [[Google Scholar](#)]
24. Gómez, E.; Pellicer, E.; Vallés, E. Influence of the bath composition and the pH on the induced cobalt–molybdenum electrodeposition. J. Electroanal. Chem. **2003**, 556, 137–145. [[Google Scholar](#)] [[CrossRef](#)]
25. Kazimierzaka, H.; Ozga, P.; Sochab, R.P. Investigation of electrochemical co-deposition of zinc and molybdenum from citrate solutions. Electrochim. Acta **2013**, 104, 378–390. [[Google Scholar](#)] [[CrossRef](#)]
26. Jung, S.M. Quantitative analysis of FeMo alloys by X-ray fluorescence spectrometry. Am. J. Anal. Chem. **2014**, 5, 766–774. [[Google Scholar](#)] [[CrossRef](#)]
27. Ma, S.; Xing, J.; Fu, H.; Yi, D.; Zhang, J.; Li, Y.; Zhang, Z.; Zhu, B.; Ma, S. Interfacial morphology and corrosion resistance of Fe–B cast steel containing chromium and nickel in liquid zinc. Corr. Sci. **2011**, 53, 2826–2834. [[Google Scholar](#)] [[CrossRef](#)]
28. Chassaing, E.; Quang, K.V.; Wiart, R. Mechanism of nickel-molybdenum alloy electrodeposition in citrate electrolytes. J. Appl. Electrochem. **1989**, 19, 839–844. [[Google Scholar](#)] [[CrossRef](#)]
29. Fukushima, H.; Akiyama, T.; Akagi, S.; Higashi, K. Role of iron-group metals in the induced codeposition of molybdenum from aqueous solution. Trans. JIM **1979**, 20, 358–364. [[Google Scholar](#)] [[CrossRef](#)]
30. Kubota, A.; Tashiro, Y.; Yamasaki, K.; Nakano, H.; Oue, S.; Kobayashi, S.; Akiyama, T.; Fukushima, H. Electrodeposition behavior and properties of iron-group metal alloys with W from ammoniacal citrate baths. Tetsu-to-Hagane **2000**, 86, 116–122. (In Japanese) [[Google Scholar](#)] [[CrossRef](#)]
31. Dear PURSHOTHAM.P.KATTI,
32. Thank you for submitting paper in IJNRD. You will be intimated for final selection & acceptance of your paper very soon.  
Your paper will undergo the normal review process of the Journal. The process normally takes 1 to 3 Days to complete depending on the number of rounds the reviews need to take place.